The American Journal of Chinese Medicine, Vol. 48, No. 6, 1–19

DOI: 10.1142/S0192415X20500731

Astragalus Polysaccharide (PG2) Suppresses Macrophage Migration Inhibitory Factor and Aggressiveness of Lung Adenocarcinoma Cells

Chien-Huang Liao,[*,a] Chen-Yin Yong,[†,a] Gi-Ming Lai,[*,‡,¶,//,**] Jyh-Ming Chow,[‡,¶] Chieh-Fang Cheng,[††] Chia-Lang Fang,[§] Pei-Chun Lin,[*] Chia-Lun Chang,[‡,¶] Yu-Mei Zheng,[‡] Shuang-En Chuang,[**] Jacqueline Whang-Peng[*,‡,//] and Chih-Jung Yao[*,¶]

[*]*Cancer Center*

[†]*Division of Oral and Maxillofacial Surgery*
Department of Dentistry

[‡]*Division of Hematology and Medical Oncology*
Department of Internal Medicine

[§]*Department of Pathology, Wan Fang Hospital*
Taipei Medical University
Taipei 11696, Taiwan

[¶]*Department of Internal Medicine*
School of Medicine, College of Medicine

[//]*Taipei Cancer Center, Taipei Medical University*
Taipei 11031, Taiwan

[**]*National Institute of Cancer Research*
National Health Research Institutes
Miaoli 35053, Taiwan

[††]*PhytoHealth Corporation*
Taipei 10547, Taiwan

Published 13 September 2020

Abstract: *Astragalus membranaceus* is the most popular traditional Chinese medicine for managing vital energy deficiency. Its injectable polysaccharide PG2 has been used for relieving cancer-related fatigue, and PG2 has immune-modulatory and anti-inflammatory effects. In this study, we explored the effects of PG2 in lung adenocarcinoma A549 and

Correspondence to: Dr. Chih-Jung Yao, Department of Internal Medicine, School of Medicine, College of Medicine, Taipei Medical University, Taipei, Taiwan. Tel: (+886) 2-29307930 (ext. 8130), Fax: (+886) 2-8663-6454, E-mail: yaochihjung@gmail.com
[a]These authors contributed equally to this work.

CL1-2 cells and investigated its anticancer activity, and the results were validated in severe combined immunodeficiency (SCID) mice. Although PG2 did not inhibit the growth of these cells, it dose-dependently suppressed their migration and invasion, accompanied by reduced vimentin and AXL and induced epithelial cadherin (E-cadherin) expression. Regarding the underlying molecular mechanism, PG2 treatment reduced the macrophage migration inhibitory factor (MIF), an inflammatory cytokine that promotes the epithelial–mesenchymal transition and aggressiveness of cancer cells. Consistent with the previous finding that MIF regulates matrix metalloproteinase-13 (MMP-13) and AMP-activated protein kinase (AMPK), treatment with PG2 reduced MMP-13 and activated AMPK in A549 and CL1-2 cells in this study. In SCID mice injected with A549 cells through the tail vein, intraperitoneal injection with PG2 reduced lung and abdominal metastases in parallel with decreased immunohistochemical staining of AXL, vimentin, MMP-13, and MIF in the tumor. Collectively, data revealed a potential application of PG2 in integrative cancer treatment through the suppression of MIF in cancer cells and their aggressiveness.

Keywords: *Astragalus membranaceus*; PG2; Lung Adenocarcinoma; Macrophage Migration Inhibitory Factor; Epithelial–Mesenchymal Transition.

Introduction

Lung cancer is the leading cause of cancer death worldwide (Torre *et al.*, 2016). The most common type of lung cancer is adenocarcinoma, accounting for approximately 40% of all lung cancer cases (Denisenko *et al.*, 2018). In addition to uncontrolled proliferation, the mobility and invasiveness of cancer cells result in metastasis, which is the most lethal aspect of cancer (Hurst and Welch, 2011). The prevention and treatment of metastasis are critical to improving clinical outcomes. The development of clinical approaches to inhibit cancer metastasis is urgently required.

The epithelial–mesenchymal transition (EMT) confers cancer cells with aggressive metastatic properties by enhancing their mobility and invasiveness (Mittal, 2018). Cancer cells undergoing EMT exhibit both morphological changes and molecular alterations, as revealed by the decreased expression of epithelial markers, such as epithelial cadherin (E-cadherin), zonula occludens protein 1 (ZO-1), and occludin, and the increased expression of mesenchymal markers, including neural cadherin (N-cadherin), vimentin, fibroblast-specific protein 1, and fibronectin (Mittal, 2018). In addition to these cytoskeleton and adhesion molecules, the invasiveness-associated receptor tyrosine kinase AXL (Lay *et al.*, 2007) has been described as an EMT marker in non-small-cell lung carcinoma (Byers *et al.*, 2013) and in other types of cancer, including esophageal squamous cell carcinoma (Zhang *et al.*, 2018), breast (Gjerdrum *et al.*, 2010), prostate (Mishra *et al.*, 2012), ovarian (Antony *et al.*, 2016), and pancreatic (Koorstra *et al.*, 2009) cancers. Downregulation of AXL in A549 and H460 lung cancer cells led to the enhanced expression of E-cadherin and the decreased expression of vimentin and N-cadherin (Byers *et al.*, 2013; Wu *et al.*, 2014), demonstrating the pivotal role of AXL in maintaining EMT.

EMT plays crucial roles in several physiological and pathological conditions and is regulated by multiple pathways (Dongre and Weinberg, 2018). The complex signaling pathways responsible for the activation of EMT in cancer cells have been extensively explored by researchers for various medical applications (Lamouille *et al.*, 2014). Growing evidence indicates that extracellular cues from the tumor microenvironment play a critical role in activating EMT. In addition to growth factor signaling, inflammatory cytokine cascades have been shown to drive the EMT of cancer cells (Lopez-Novoa and Nieto, 2009; Tsai and Yang, 2013; Mittal, 2018). Among these, the proinflammatory cytokine macrophage migration-inhibitory factor (MIF) has been shown to induce EMT in human pancreatic cancer (Funamizu *et al.*, 2013) and glioblastoma (Guo *et al.*, 2017) cells. In lung adenocarcinoma cells, MIF is implicated in EMT induction by TGF-β (Keshamouni *et al.*, 2009) or in response to ionizing radiation (Youn *et al.*, 2015). Studies have shown the contribution of MIF to the anchorage independence, mobility, and invasive potential of A549 lung adenocarcinoma cells (Rendon *et al.*, 2007; Winner *et al.*, 2008) and have further demonstrated its negative regulation of AMP-activated protein kinase (AMPK) activity in non-small-cell lung carcinoma cells (Brock *et al.*, 2012). High expression of MIF has been found in non-small-cell lung carcinoma (Brock *et al.*, 2012; Youn *et al.*, 2015) and various types of tumors, including melanoma, glioblastoma, and prostate, colon, and pancreatic cancers (Funamizu *et al.*, 2013; Guo *et al.*, 2017). It is an integral component of the host inflammatory response and directly or indirectly promotes the production of many proinflammatory cytokines, for example, IL-6, IL-1β, IL-8, and TNF-α (Calandra and Roger, 2003). Moreover, MIF regulates matrix metalloproteinase-13 (MMP-13) (Onodera *et al.*, 2002), which has been detected in early pulmonary invasive adenocarcinomas and is a potential target for molecular imaging of lung cancer (Salaun *et al.*, 2015). Targeting the MIF cascade constitutes a potential strategy for inhibition of both inflammation and EMT.

PG2 is an injectable sterile polysaccharide isolated from *Astragalus membranaceus*. Its benefits in relieving cancer-related fatigue and improving quality of life in patients with advanced cancer have been demonstrated in a clinical study (Chen *et al.*, 2012). Thus, the Taiwan Food and Drug Administration (TFDA) has approved PG2 for treating cancer-related fatigue. Recent studies have shown the immune-modulatory and anti-inflammatory activities of PG2 (Bamodu *et al.*, 2019; Huang *et al.*, 2019) and suggested its anticancer effects (Bamodu *et al.*, 2019; Phacharapiyangkul *et al.*, 2019). In this study, we explored the effects of PG2 on the MIF-EMT cascade in lung adenocarcinoma cells to further investigate its activity against cancer. The effects of PG2 on MIF and related EMT markers, MMP, and the aggressiveness of lung adenocarcinoma cells were investigated both *in vitro* models and in severe combined immunodeficiency (SCID) mice injected with adenocarcinoma cells through the tail vein.

Materials and Methods

Cell Culture

The human lung adenocarcinoma cell lines A549 (*LKB1* mutant), CL1-0 (*LKB1* wild-type), and CL1-2 (*LKB1* wild-type) were maintained in RPMI 1640 medium (Gibco, CA, USA).

Luciferase-expressing A549 cells (A549-Luc) were cultured in DMEM (Gibco) containing 500 μg/mL Geneticin™ Selective Antibiotic (G418 Sulfate) (Thermo Fisher Scientific, IL, USA). All the cell culture media were supplemented with 10% fetal bovine serum (Corning, NY, USA), 1 × penicillin–streptomycin–glutamine (Corning), and 1 × nonessential amino acids (Corning). Cells were cultured at 37°C in a water-jacketed 5% CO_2 incubator. A549 cells were purchased from the Bioresource Collection and Research Center (Hsinchu, Taiwan), and CL1-0 and CL1-2 cells were kindly provided by Dr. Shine-Gwo Shiah (National Institute of Cancer Research, National Health Research Institutes, Miaoli, Taiwan). A549-Luc cells were kindly provided by Dr. Bing-Ying Ho (Department of Anesthesiology, Wan Fang Hospital, Taipei Medical University, Taipei, Taiwan).

Reagents and Chemicals

The lyophilized powder of injectable *Astragalus* polysaccharide (APS, named PG2) was provided by PhytoHealth Corporation, Taiwan. Detailed information on PG2 injection is provided at https://www.phytohealth.com.tw/en/product/8/product_detail. The PG2 powder was dissolved in sterile saline to prepare a 50 mg/mL stock solution, which was then aliquoted and stored at −20°C for no more than 3 months. On the day of an experiment, it was diluted in sterile culture medium immediately before use. Sulforhodamine B (SRB) and trichloroacetic acid were purchased from Sigma (St. Louis, MO, USA).

Assessment of Cell Viability

Cells were seeded in a 96-well plate for 24 h (A549 cells, 1500 cells/well; CL1-0 and CL1-2 cells, 1700 cells/well) and then treated with drugs or sterile culture medium for 72 h. Cell viability was measured using the SRB binding assay. Briefly, cells were fixed with 10% trichloroacetic acid and incubated for 1 h at 4°C. The plates were then washed twice with tap water and air-dried. The dried plates were stained with 80 μL 0.4% (w/v) SRB prepared in 1% (v/v) acetic acid for 30 min at room temperature. The plates were rinsed quickly twice with 1% acetic acid to remove unbound SRB and then air-dried until no moisture was visible. The bound dye was solubilized in 20 mM Tris base (200 μL/well) for 5 min on a shaker. Optical densities were read on a microplate reader (ELx800; BioTek, Winooski, VT, USA) at 570 nm. The optical density is directly proportional to the cell number over a wide range.

In Vitro Migration and Invasion Analysis using Boyden Chamber Assay

In vitro cell migration was assessed by using the Falcon® permeable support for 24-well plate with 8.0- μm transparent PET membrane (#353097, Corning, NY, USA), and cell invasion was assessed by using the Corning® BioCoat™ Matrigel® invasion chamber with 8.0- μm PET membrane in 24-well plate (#354480, Corning, MA, USA). After pretreatment with PG2 for 72 h, cancer cell suspensions were seeded in the upper compartment

of the Transwell chamber at a cell density of 6×10^4 cells/mL (A549, CL1-0, and CL1-2 cells) in serum-free medium (0.35 mL/well and 0.5 mL/well for migration and invasion assays, respectively). The lower chamber was filled with medium containing 10% serum. Plates were incubated for 24 h at 37°C in 5% CO_2. After 24 h of incubation, the medium was removed, and the filter membrane was fixed with methanol for 2 min. Subsequently, cells on the upper surface of the membrane were scraped, and the remaining cells that migrated to the lower chamber were stained with 0.4% crystal violet (Sigma-Aldrich). The migrated/invaded cancer cells were then visualized and counted in five different visual fields at 100-fold magnification using an inverted microscope.

Images of Migrated/Invaded Cells

The crystal violet-stained migrated/invaded cells were photographed using a digital microscope camera (PAXcam2+ , Villa Park, IL, USA) adapted to an inverted microscope (CKX31; Olympus, Tokyo, Japan) at 10 × objective lens magnification.

Western Blotting

After cells were seeded in 10-cm dishes at a density of 3.5×10^5 (A549 cells) or 3.8×10^5 (CL1-0 and CL1-5 cells) cells/dish for 24 h, they were then treated with agents as described in the figure legends for 72 h. On the day of cell harvesting, whole-cell lysates were extracted with 1 × radioimmunoprecipitation lysis buffer (Millipore, Billerica, MA, USA) containing 1 × tyrosine phosphatase inhibitor cocktail (FC0020-0001; BIONOVAS, Toronto, Canada), 1 × protease inhibitor cocktail, full-range (FC0070-0001, BIONOVAS), and 1 × serine/threonine phosphatase inhibitor cocktail (FC0030-0001, BIONOVAS). The protein extracts were resolved by sodium dodecyl sulfate–polyacrylamide gel electrophoresis and subsequently transferred to polyvinylidene difluoride membrane (GE Healthcare, Pittsburgh, PA, USA) through electroblotting. The membranes were blocked with 3% bovine serum albumin in TBST buffer (Tris-buffered saline with Tween 20, 25 mM Tris-HCl, 125 mM NaCl, 0.1% Tween 20) for 1 h at room temperature and incubated with primary antibody overnight at 4°C and then with horseradish peroxidase-conjugated secondary antibody for 1 h at room temperature. Intensive wash with TBST buffer was performed after each time of incubation. Immune complexes were visualized using enhanced chemiluminescence (ECL) reagent plus (Perkin Elmer, Waltham, MA, USA), and light-producing reactions were captured with X-ray film.

Antibodies

Primary antibodies used for Western blotting were as follows: phospho-AMPKα (Thr172, #2535), AXL (#8661) and E-cadherin (#3195) purchased from Cell Signaling (Danvers, MA, USA) as well as vimentin (ab92547), MMP-13 (ab39012), MIF (ab65869), and GAPDH (ab8245) purchased from Abcam (Cambridge, MA, USA). Primary antibodies used for immunohistochemical staining were as follows: AXL (#8661) purchased

from Cell Signaling (Danvers, MA, USA); vimentin (ab16700) and MIF (ab55445) purchased from Abcam; and MMP-13 (#701287) purchased from Thermo Fisher Scientific.

Experimental Xenograft Murine Metastasis Model

Five-week-old male NOD/SCID mice were purchased from BioLASCO Taiwan (Taipei, Taiwan). This study was conducted in accordance with the recommendations of the animal care guidelines of the Laboratory Animal Center of Taipei Medical University. The study protocol was approved by the Laboratory Animal Center of Taipei Medical University (approval no: LAC-2018-0175). All mice were injected with A549-Luc cells through the tail vein (4×10^5 cells in 0.1 mL PBS). From the second day, PG2 (10, 40, and 160 mg/kg body weight, $n = 6$/each group) or saline ($n = 6$) was injected intraperitoneally trice weekly. Tumor metastasis was analyzed after 5 weeks. Mice were injected with D-luciferin and imaged for 5 min by using the Xenogen IVIS-200 System (PerkinElmer, MA, USA). After tissue fixation in formalin solution, the numbers of lung metastases were confirmed under a dissecting microscope. The lungs were further subjected to hematoxylin and eosin (H&E) staining.

Immunohistochemistry Assay

Immunohistochemistry (IHC) was performed as previously reported (Huang *et al.*, 2016). The lung tissues of mice were embedded in paraffin for the immunohistochemical staining of AXL, vimentin, MIF, and MMP-13. The images of IHC were acquired using a hamamatsu nanozoomer 2.0-HT digital slide scanner (Hamamatsu Photonics Deutschland GmbH, Ammersee, Germany).

Statistical Analysis

Quantitative data were statistically evaluated using ANOVA, followed by Dunnett's *t*-test. $p < 0.05$ was considered statistically significant. A single asterisk (*) indicates $p < 0.05$; double asterisks (**) indicate $p < 0.01$; and triple asterisks (***) indicate $p < 0.001$.

Results

PG2 Inhibits the Migration and Invasion of A549 Lung Adenocarcinoma Cells

To explore the direct effect of PG2 on lung cancer cells, we first tested the effect of PG2 on the proliferation of A549 lung adenocarcinoma cells. As shown in Fig. 1A, PG2 at a dose within 1000 μg/mL did not affect the proliferation of A549 cells. In addition to intensive proliferation, A549 cells are aggressively invasive (Huang *et al.*, 2017) and exhibit high endogenous expression of the EMT markers AXL and vimentin (Wu *et al.*, 2014). Thus, we then investigated if 72-h treatment with PG2 changed the migration and invasiveness of A549 cells. PG2-treated cells were examined through Transwell assays, as described in the

Materials and Methods section; the results showed that PG2 dose-dependently suppressed the migration of A549 cells (Figure 1B). Treatment with PG2 at a dose of 500 μg/mL inhibited 68.6% of cell migration (Fig. 1B). Similar results were found in the cell invasion assay (Fig. 1C). Treatment with PG2 at a dose of 500 μg/mL inhibited 72.2% of A549 cell

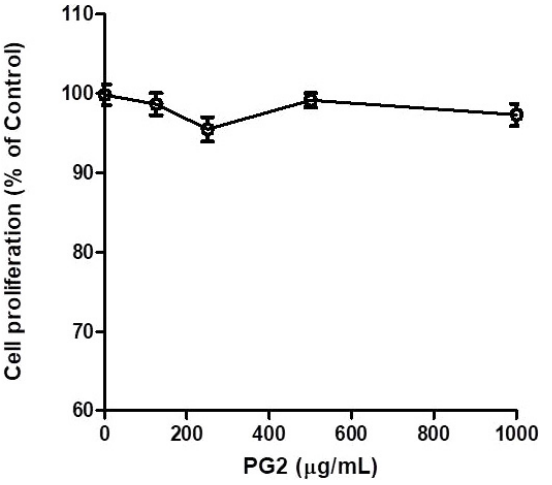

(A)

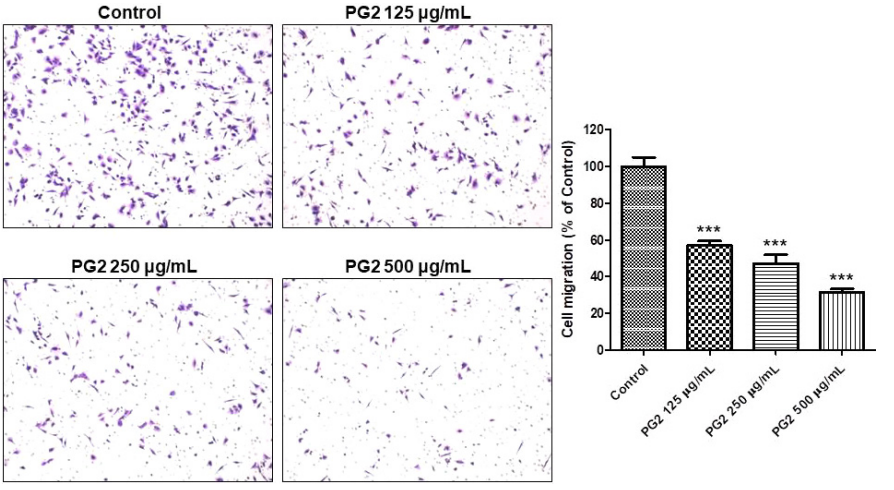

(B)

Figure 1. Effects of 72-h treatment with PG2 on the proliferation and migration and invasion abilities of A549 cells. (A) The viability of A549 cells determined through the SRB staining assay. (B) The migration ability of A549 cells assessed using an 8.0- μm transparent PET membrane in the Transwell assay, as described in the Materials and Methods section. (C) The invasion ability of A549 cells assessed using a Matrigel™-coated 8.0- μm PET membrane in Transwell in the Transwell assay, as described in the Materials and Methods section. The data are expressed as means ± standard errors of five replicates (migration and invasion) or six replicates (cell proliferation). $^{**}p < 0.01$; $^{***}p < 0.001$, compared with the control.

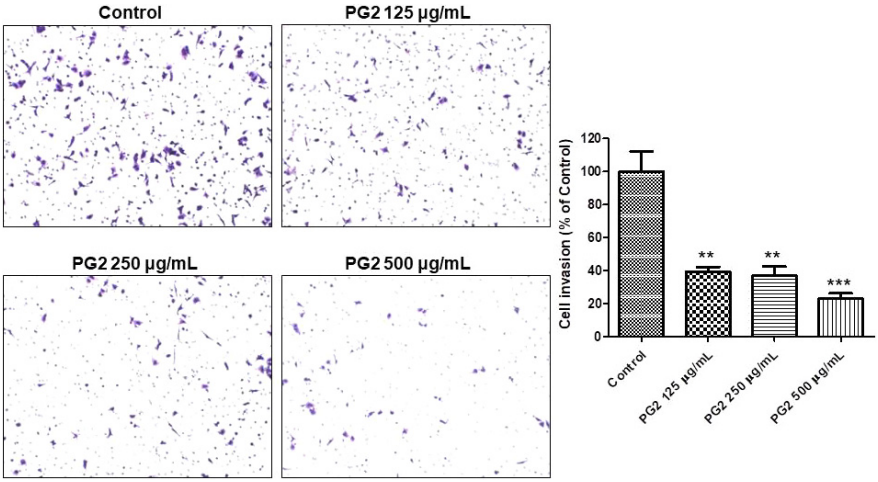

(C)

Figure 1. (*Continued*)

invasion (Fig. 1C). Although PG2 did not affect the proliferation of A549 cells at a dose within 1000 μg/mL, it suppressed their aggressiveness in terms of migration and invasion potential.

PG2 Suppresses MIF Accompanied by Inhibition of EMT in A549 Cells

To elucidate molecular mechanisms underlying the inhibitory effects of PG2 on the migration and invasion of A549 cells, we examined changes in EMT markers, such as AXL and vimentin, which are highly expressed in these cells. As shown in Fig. 2A, 72-h treatment with PG2 substantially suppressed the protein levels of AXL and vimentin. To further delineate the action mechanism of PG2 against the aggressiveness of A549 cells with regard to its recently implicated anti-inflammatory role (Kuo *et al.*, 2015), we examined changes in MIF, an important EMT promoting proinflammatory cytokine (Keshamouni *et al.*, 2009; Funamizu *et al.*, 2013; Youn *et al.*, 2015; Guo *et al.*, 2017), in PG2-treated A549 cells. As expected, PG2 reduced the MIF protein level in a dose-dependent manner, accompanied by the induction of the epithelial marker E-cadherin (Fig. 2B).

The degradation of the extracellular matrix by MMPs is required for the invasion of cancer cells. MMP-13 can be upregulated by MIF (Onodera *et al.*, 2002) and has been detected in early pulmonary invasive adenocarcinomas (Salaun *et al.*, 2015). In this study, we then determined if MMP-13 decreases along with the suppression of MIF. The result showed a significant decrease in the MMP-13 protein level in A549 cells after treatment with PG2 (Fig. 2C). Moreover, inhibition of MIF has been shown to restore the activated (phosphorylated) AMPK (p-AMPK) in A549 cells (Brock *et al.*, 2012). Consistently, we also found an increase in p-AMPK in A549 cells upon inhibition of MIF by treatment with PG2 (Fig. 2D).

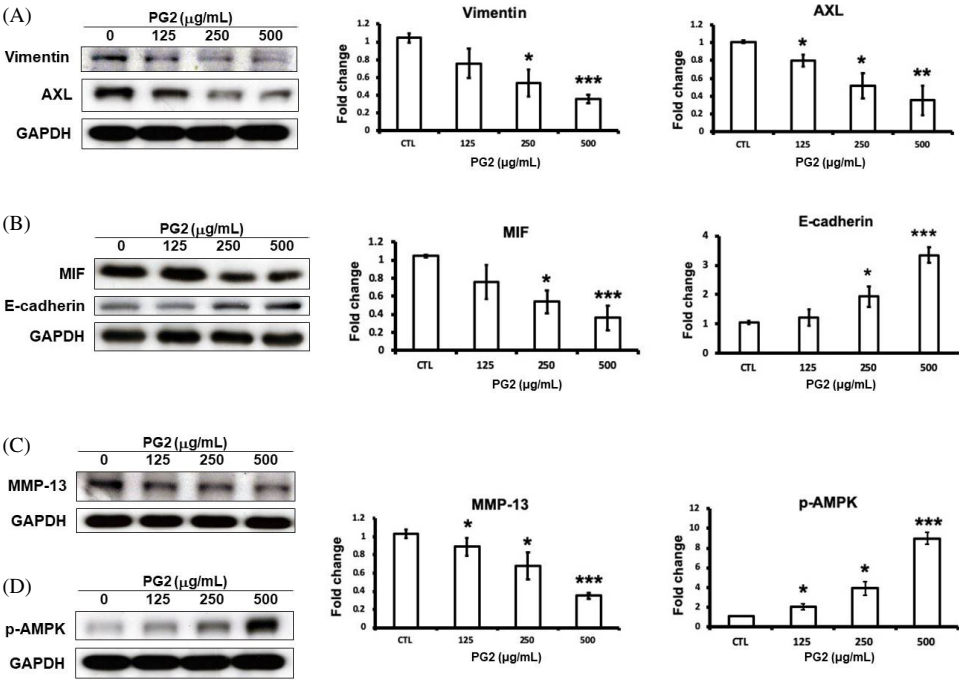

Figure 2. Effects of PG2 on the vimentin, AXL, MIF, E-cadherin, MMP-13, and phospho-AMPK (p-AMPK) protein levels of A549 cells. Cells were treated with the indicated concentrations of PG2 for 72 h. Cell lysates were analyzed through Western blotting for determining the protein levels of (A) vimentin and AXL, (B) MIF and E-cadherin, (C) MMP-13, and (D) phospho-AMPK (p-AMPK), with GAPDH used as the loading control. Data presented are the representative Western blotting images and average fold changes in protein levels of three independent experiments. Values represent means ± standard errors (n = 3). $*p < 0.05$; $**p < 0.01$; $***p < 0.001$, compared with the control (CTL).

These results indicate the crucial role of MIF suppression in the effects of PG2 against the aggressiveness of A549 cells.

PG2 Inhibits the Migration and Invasion of the Aggressive Lung Adenocarcinoma Sub-line CL1-2

We evaluated the effects of PG2 in another aggressive lung adenocarcinoma cell line CL1-2, an invasive subpopulation of CL1-0 cells selected through Transwell invasion screening and single-colony selection (Chu *et al.*, 1997). Similar to results observed in A549 cells, PG2 did not affect the proliferation of CL1-2 cells (Fig. 3A). In the Transwell assay, the migration capability of CL1-2 cells was drastically elevated in comparison with that of CL1-0 cells (Fig. 3B). Although the proliferation of CL1-2 cells was not affected by 72 h-treatment with PG2, their migration ability was substantially inhibited in a dose-dependent manner (Fig. 3B). Compared with the CL1-2 control, the migration rate was reduced to 45% in CL1-2 cells preincubated with 500 μg/mL PG2 (Fig. 3B). The invasive ability of

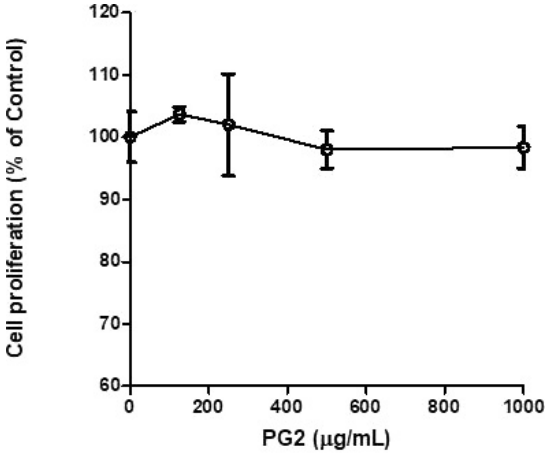

(A)

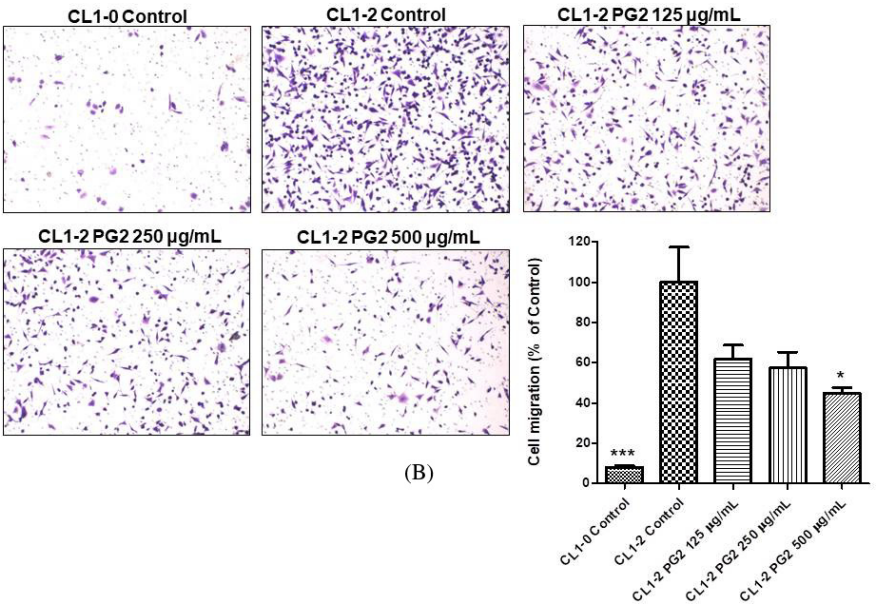

(B)

Figure 3. Effects of 72-h treatment with PG2 on the proliferation and migration and invasion abilities of CL1-2 cells. (A) The viability of CL1-2 cells determined using the SRB staining assay. (B) The migration ability of CL1-0 and CL1-2 cells was assessed using an 8.0-μm transparent PET membrane in the Transwell assay, as described in the Materials and Methods section. (C) The invasion ability of CL1-0 and CL1-2 cells was assessed using a Matrigel™-coated 8.0-μm PET membrane in the Transwell assay, as described in the Materials and Methods section. The data are expressed as means ± standard errors of five replicates (migration and invasion) or three replicates (cell proliferation). $*p < 0.05$; $**p < 0.01$; $***p < 0.001$, compared with the CL1-2 control.

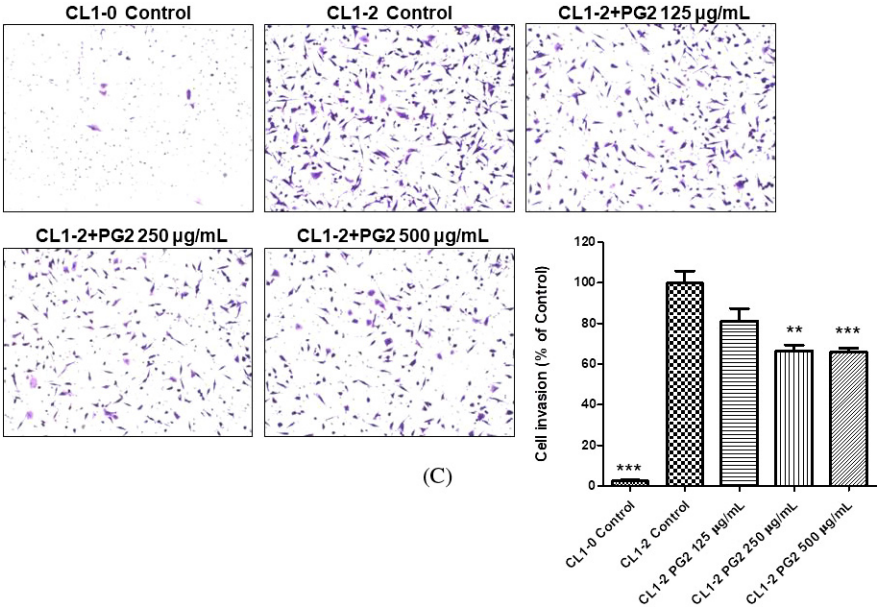

Figure 3. (*Continued*)

CL1-2 cells was also much higher than that of CL1-0 cells (Fig. 3C). Similarly, the invasion rate was significantly suppressed in PG2-pretreated CL1-2 cells (Fig. 3C). Treatment with PG2 at a dose of 500 μg/mL resulted in a 34.2% reduction of the invasion rate (Fig. 3C).

In addition to reducing the aggressiveness of A549 cells, PG2 reduced the migration and invasiveness capacity of the selected aggressive sub-line CL1-2 cells.

PG2 Suppresses Elevated MIF and EMT Markers in CL1-2 Cells

Consistent with the finding of elevated aggressiveness, we found that the MIF level in CL1-2 cells was much higher than that in CL1-0 cells, and the MIF level could be markedly decreased by 72 h-treatment with PG2 (Fig. 4A). Similar to the result of Lai *et al.* (Lay *et al.*, 2007), the AXL level was much higher in CL1-2 cells than in CL1-0 cells (Figure 4B). Moreover, higher vimentin and lower E-cadherin levels were observed in CL1-2 cells (Figure 4B). In accordance with the suppression of cell migration and invasion shown in Figure 3B and 3C, 72-h treatment with PG2 reduced AXL and vimentin levels, along with the induction of E-cadherin expression, in CL1-2 cells (Fig. 4B). Consistent with the finding in A549 cells, the elevated MIF level in CL1-2 cells was accompanied by the decreased activation of AMPK (Figure 4B) and increased MMP-13 levels (Fig. 4C) than those in CL1-0 cells. Treatment with PG2 restored AMPK activation and reduced the MMP-13 level in CL1-2 cells (Figs. 4B and 4C). Figure 4 shows that the inhibition of MIF by PG2 in CL1-2 cells not only reduces EMT markers (AXL and vimentin) but also represses MMP-13 and restores AMPK activation.

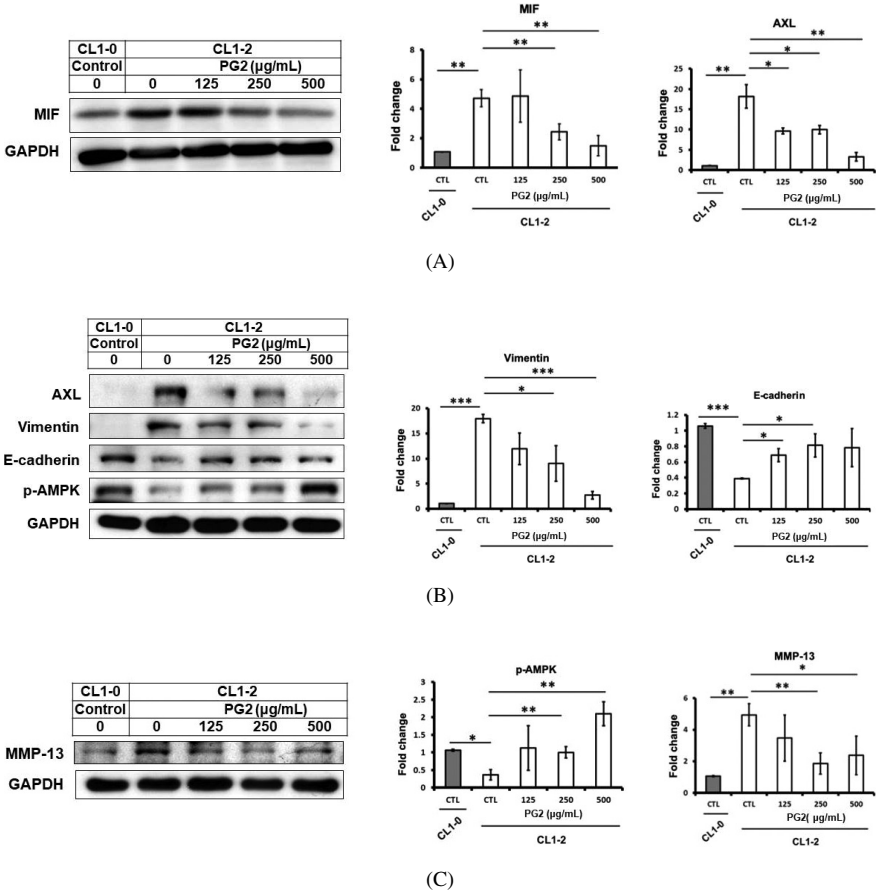

Figure 4. Effects of PG2 on the MIF, AXL, vimentin, E-cadherin, phospho-AMPK (p-AMPK), and MMP-13 protein levels of CL1-2 cells. CL1-0 and CL1-2 cells were treated with the indicated concentrations of PG2 for 72 h. Cell lysates were analyzed through Western blotting for determining the protein levels of (A) MIF, (B) AXL, vimentin, E-cadherin, and phospho-AMPK (p-AMPK), and (C) MMP-13, with GAPDH used as the loading control. Data presented are the representative Western blotting images and average fold changes in protein levels of three independent experiments. Values represent the means ± standard errors (n = 3). $*p < 0.05$; $**p < 0.01$; $***p < 0.001$, compared with the CL1-2 control (CTL).

PG2 Reduces Metastasis and Immunohistochemical Staining of Tumor MIF and EMT Markers in SCID Mice Injected with A549 Cells

To further demonstrate the antimetastatic property of PG2 *in vivo*, we injected luciferase-expressing A549 (A549-Luc) cells into the tail vein of a murine (NOD/SCID mice) metastasis model. After being intraperitoneally injected with saline or PG2 (10, 40, and 160 mg/kg) for 48 h, NOD/SCID mice were intravenously injected with A549-Luc cells through the tail vein. Subsequently, mice were intraperitoneally injected with PG2 thrice a week, and mice were imaged using the IVIS imaging system at week 5 (Fig. 5A). After

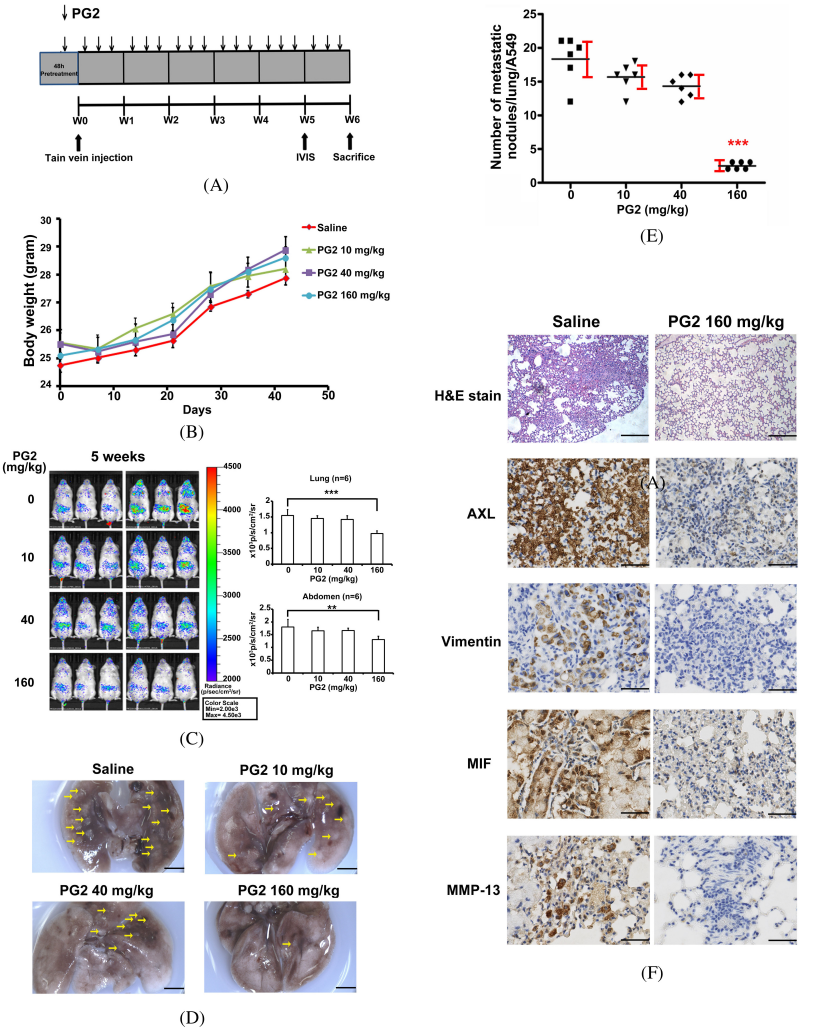

Figure 5. PG2 suppresses lung cancer metastasis in a mouse xenograft model. (A) Schematic overview of PG2 administration. First, saline or PG2 (10, 40, and 160 mg/kg) was intraperitoneally injected into male NOD/SCID mice. After 48-h injection of PG2, all mice were intravenously injected with A549 cells expressing luciferase (A549-Luc, 4×10^5) through the tail vein. PG2 was injected thrice a week. Metastasis of A549-Luc cells was monitored using the IVIS imaging system at indicated time intervals. All mice were sacrificed at the 6th week, and lung segments were fixed in formalin. (B) A549-Luc cells were injected intravenously into NOD/SCID mice through the tail vein. Mice were injected intraperitoneally trice weekly with saline or 10, 40, and 160 mg/kg PG2. Body weights of all treatment mice are shown. The data are presented as means $\pm$ standard errors. (C) The luciferase activity of all mice injected with A549-Luc cells was detected using a noninvasive imaging system (IVIS imaging system, Xenogen) at week 5. Synchronized images were quantified (right panel). The data are presented as means $\pm$ standard errors. ***$p < 0.001$, **$p < 0.01$, compared with the saline-treated control. (D) Gross pictures of the lungs are shown. The arrowhead indicates macroscopic lesions (scale bar: 5 mm). (E) The quantified numbers of lung metastatic nodules on the surface. The data are expressed as means $\pm$ standard errors. ***$p < 0.001$, compared with the saline-treated control. (F) Lung tissues were detected by H&E staining and immunohistochemical staining with anti-AXL, anti-vimentin, anti-MIF, or anti-MMP-13 antibody, and the representative results are shown. Scale bar for H&E staining is 100 μm; Scale bar for immunohistochemical staining is 50 μm.

PG2 injection for 6 weeks, the results revealed that PG2 did not affect the body weight of NOD/SCID mice (Figure 5B). As shown in Fig. 5C, IVIS imaging results revealed that all saline-treated mice had high fluorescent intensity, representing tumor foci in various organs, including the lung and abdominal organs. By contrast, PG2 (160 mg/kg)-treated mice showed significantly reduced fluorescent intensity of the lung and abdominal area, suggesting that treatment with 160 mg/kg PG2 inhibited A549-Luc cell metastasis. After PG2 treatment for 6 weeks, mice were sacrificed, and the number of lung metastatic nodules on the surface was quantified through microscopic examination (Fig. 5D). This examination confirmed the antimetastatic property of PG2 (Figure 5E). H&E staining revealed that the tumor section from saline-treated mice showed multiple foci of large aggregates of tumor cells. By contrast, tumor foci were less severe in the PG2 (160 mg/kg)-treated group (Fig. 5F). In IHC analysis, PG2 markedly reduced the protein levels of AXL, vimentin, MIF, and MMP-13 (Fig. 5F). These results indicate the antimetastatic potential of PG2 *in vivo* and support our *in vitro* finding.

Discussion

The botanical-derived drug PG2 contains a mixture of APSs purified from the roots of *A. membranaceus*. Historically, *A. membranaceus* is a widely used Chinese herbal medicine for managing vital energy deficiency (McKenna *et al.*, 2002). PG2 has been demonstrated to relieve cancer-related fatigue among patients with advanced cancer (Chen *et al.*, 2012), and this indication has been approved by TFDA. Modern pharmacological research has shown the various biological properties of APSs, including immunomodulatory, anti-inflammatory, and antitumor effects (Jin *et al.*, 2014). Recently, the Good Manufacturing Practice (GMP)-grade preparation of APSs (i.e., PG2) also has been implicated in immunomodulation and anti-inflammation by Kuo *et al.* (Kuo *et al.*, 2015). Growing evidence has demonstrated the close interplay between inflammatory microenvironment and cancer progression (Keibel *et al.*, 2009; Gao *et al.*, 2014). In line, our results show that PG2 suppresses the proinflammatory cytokine MIF and inhibits the EMT in A549 lung adenocarcinoma cells.

MIF is recognized as a molecular link between inflammation and cancer (Conroy *et al.*, 2010). Its EMT promoting effect has been reported for glioblastoma (Guo *et al.*, 2017) and pancreatic cancer (Funamizu *et al.*, 2013). Rendon *et al.* showed that MIF regulates lung adenocarcinoma cell migration and invasion (Rendon *et al.*, 2007). In agreement with these reports, our results demonstrated that PG2 caused the suppression of MIF, accompanied by the inhibition of EMT and migration and invasion abilities in A549 cells, a lung adenocarcinoma cell line established from a Caucasian male lung adenocarcinoma patient. Moreover, similar inhibitory effects of PG2 on MIF and EMT features were also shown in CL1-2 cells, an aggressive sub-line of CL1-0, which was originally established from a 64-year-old Taiwan male patient with poorly differentiated adenocarcinoma (Chu *et al.*, 1997). In support of the association between MIF and EMT, higher MIF levels were found in the aggressive CL1-2 sub-line exhibiting the higher expression of EMT markers than in the parental CL1-0 cell line.

In addition to being a novel EMT marker in lung adenocarcinoma cells, AXL is a receptor tyrosine kinase (Byers *et al.*, 2013). Its aberrant overexpression is correlated with drug resistance (Lay *et al.*, 2007; Byers *et al.*, 2013; Wu *et al.*, 2014) and poor clinical outcomes (Zhang *et al.*, 2018). The current study showed the inhibitory effects of PG2 on AXL; the potential of PG2 in alleviating drug resistance and improving prognosis should be explored in a future study.

In contrast to the AMPK-activating properties of MIF in nontransformed cells, Brock *et al.* reported that MIF inhibits the steady-state phosphorylation of AMPK in *LKB1* wild-type and *LKB1* mutant human non–small-cell lung carcinoma cell lines (Brock *et al.*, 2012). In agreement, our results showed that PG2 caused the activation of AMPK along with the inhibition of MIF in *LKB1* mutant A549 and *LKB1* wild-type CL1-2 cells. Also, CL1-2 cells with higher MIF levels had lower AMPK activation than the CL1-0 cells with lower MIF. Because AMPK-activating phenotypes in lung adenocarcinoma are tumor-suppressive (Brock *et al.*, 2012), the restored activation of AMPK might also participate in the anti-invasion/migration effect of PG2.

Consistent with the important role of MMP-13 in lung cancer metastasis (Jiang *et al.*, 2015; Salaun *et al.*, 2015), the aggressive CL1-2 sub-line showed higher MMP-13 expression than the parental CL1-0 cell line. Inhibition of MIF has been shown to down-regulate MMP-13 expression in humans and rats (Ohkawara *et al.*, 2002; Pan *et al.*, 2011). In line with this finding, the current study showed that decreases in MIF levels in PG2-treated CL1-2 and A549 cells were accompanied by MMP-13 reduction. This inhibition of MMP-13 is speculated to play an important role in PG-2-mediated anti-invasion effect in lung adenocarcinoma cells in both the *in vitro* Transwell assay and *in vivo* xenograft murine metastasis model.

In addition to promoting EMT, MIF induces VEGF expression in cancer cells and stimulates tumor angiogenesis (Nishihira *et al.*, 2003; Xu *et al.*, 2008). Its expression in non-small-cell lung cancer is closely associated with the tumor levels of angiogenic CXC chemokines and vessel density (White *et al.*, 2003). Moreover, MIF impairs the antitumor immune response, promoting cancer progression (Otvos *et al.*, 2016; Balogh *et al.*, 2018). Regarding the inhibitory effect of PG2 on MIF levels in cancer cells, its potential in modulating angiogenesis and the antitumor immune response in immunocompetent syngeneic mouse model should be evaluated.

MIF is also produced by a variety of cells, including immune and epithelial cells (Calandra and Roger, 2003; Funamizu *et al.*, 2013). By upregulating Toll-like receptor 4, it promotes the production of many proinflammatory cytokines, including IL-6, IL-1β, IL-8, and TNF-α (Calandra and Roger, 2003; Funamizu *et al.*, 2013). The association between IL-6, IL-1β, or TNF-α and fatigue in cancer patients has been reported in several studies (Myers, 2008; Eyob *et al.*, 2016; Kolak *et al.*, 2017). The inhibitory effect PG2 on MIF levels found in this study might be involved in the cancer-related fatigue relieving effect of PG2 reported by Chen *et al.* (Chen *et al.*, 2012). In addition to this approved indication, our results indicate the potential application of PG2 in integrative cancer treatment. Additional preclinical studies are warranted for the successful design of future clinical trials.

Acknowledgments

This study was supported by a joint grant from Wan Fang Hospital, Taipei Medical University, and PhytoHealth Corporation, Taipei, Taiwan (Grant W397); Health and Welfare Surcharge of tobacco products (MOHW108-TDU-B-212-124020); and Ministry of Science and Technology, Taiwan (MOST107-2314-B-038-080-MY2). The authors would like to thank PhytoHealth Corporation (Taipei, Taiwan) for providing the lyophilized powder of injectable APS (PG2). This manuscript was edited by Wallace Academic Editing.

References

Antony, J., T.Z. Tan, Z. Kelly, J. Low, M. Choolani, C. Recchi, H. Gabra, J.P. Thiery and R.Y. Huang. The GAS6-AXL signaling network is a mesenchymal (Mes) molecular subtype-specific therapeutic target for ovarian cancer. *Sci. Signal.* 9: ra97, 2016.

Balogh, K.N., D.J. Templeton and J.V. Cross. Macrophage Migration Inhibitory Factor protects cancer cells from immunogenic cell death and impairs anti-tumor immune responses. *PLoS One* 13: e0197702, 2018.

Bamodu, O.A., K.T. Kuo, C.H. Wang, W.C. Huang, A.T.H. Wu, J.T. Tsai, K.Y. Lee, C.T. Yeh and L.S. Wang. Astragalus polysaccharides (PG2) enhances the M1 polarization of macrophages, functional maturation of dendritic cells, and T cell-mediated anticancer immune responses in patients with lung cancer. *Nutrients* 11: 2019.

Brock, S.E., B.E. Rendon, K. Yaddanapudi and R.A. Mitchell. Negative regulation of AMP-activated protein kinase (AMPK) activity by macrophage migration inhibitory factor (MIF) family members in non-small cell lung carcinomas. *J. Biol. Chem.* 287: 37917–37925, 2012.

Byers, L.A., L. Diao, J. Wang, P. Saintigny, L. Girard, M. Peyton, L. Shen, Y. Fan, U. Giri, P.K. Tumula, M.B. Nilsson, J. Gudikote, H. Tran, R.J. Cardnell, D.J. Bearss, S.L. Warner, J.M. Foulks, S.B. Kanner, V. Gandhi, N. Krett, S.T. Rosen, E.S. Kim, R.S. Herbst, G.R. Blumenschein, J.J. Lee, S.M. Lippman, K.K. Ang, G.B. Mills, W.K. Hong, J.N. Weinstein, Wistuba, II, K.R. Coombes, J.D. Minna and J.V. Heymach. An epithelial-mesenchymal transition gene signature predicts resistance to EGFR and PI3K inhibitors and identifies Axl as a therapeutic target for overcoming EGFR inhibitor resistance. *Clin. Cancer Res.* 19: 279–290, 2013.

Calandra, T. and T. Roger. Macrophage migration inhibitory factor: A regulator of innate immunity. *Nat. Rev. Immunol.* 3: 791–800, 2003.

Chen, H.W., I.H. Lin, Y.J. Chen, K.H. Chang, M.H. Wu, W.H. Su, G.C. Huang and Y.L. Lai. A novel infusible botanically-derived drug, PG2, for cancer-related fatigue: A phase II double-blind, randomized placebo-controlled study. *Clin. Invest. Med.* 35: E1–11, 2012.

Chu, Y.W., P.C. Yang, S.C. Yang, Y.C. Shyu, M.J. Hendrix, R. Wu and C.W. Wu. Selection of invasive and metastatic subpopulations from a human lung adenocarcinoma cell line. *Am. J. Respir. Cell Mol. Biol.* 17: 353–360, 1997.

Conroy, H., L. Mawhinney and S.C. Donnelly. Inflammation and cancer: macrophage migration inhibitory factor (MIF)–the potential missing link. *QJM* 103: 831–836, 2010.

Denisenko, T.V., I.N. Budkevich and B. Zhivotovsky. Cell death-based treatment of lung adenocarcinoma. *Cell Death Dis.* 9: 117, 2018.

Dongre, A. and R.A. Weinberg. New insights into the mechanisms of epithelial-mesenchymal transition and implications for cancer. *Nat. Rev. Mol. Cell Biol.* 2018.

Eyob, T., T. Ng, R. Chan and A. Chan. Impact of chemotherapy on cancer-related fatigue and cytokines in 1312 patients: a systematic review of quantitative studies. *Curr. Opin. Support Palliat. Care* 10: 165–179, 2016.

Funamizu, N., C. Hu, C. Lacy, A. Schetter, G. Zhang, P. He, J. Gaedcke, M.B. Ghadimi, T. Ried, H. G. Yfantis, D.H. Lee, J. Subleski, T. Chan, J.M. Weiss, T.C. Back, K. Yanaga, N. Hanna, H.R. Alexander, A. Maitra and S.P. Hussain. Macrophage migration inhibitory factor induces epithelial to mesenchymal transition, enhances tumor aggressiveness and predicts clinical outcome in resected pancreatic ductal adenocarcinoma. *Int. J. Cancer* 132: 785–794, 2013.

Gao, F., B. Liang, S.T. Reddy, R. Farias-Eisner and X. Su. Role of inflammation-associated microenvironment in tumorigenesis and metastasis. *Curr. Cancer Drug Targets* 14: 30–45, 2014.

Gjerdrum, C., C. Tiron, T. Hoiby, I. Stefansson, H. Haugen, T. Sandal, K. Collett, S. Li, E. McCormack, B.T. Gjertsen, D.R. Micklem, L.A. Akslen, C. Glackin and J.B. Lorens. Axl is an essential epithelial-to-mesenchymal transition-induced regulator of breast cancer metastasis and patient survival. *Proc. Natl. Acad. Sci. U. S. A.* 107: 1124–1129, 2010.

Guo, X., S. Xu, X. Gao, J. Wang, H. Xue, Z. Chen, J. Zhang, X. Guo, M. Qian, W. Qiu and G. Li. Macrophage migration inhibitory factor promotes vasculogenic mimicry formation induced by hypoxia via CXCR4/AKT/EMT pathway in human glioblastoma cells. *Oncotarget* 8: 80358–80372, 2017.

Huang, C.W., W.C. Hsieh, S.T. Hsu, Y.W. Lin, Y.H. Chung, W.C. Chang, H. Chiu, Y.H. Lin, C.P. Wu, T.C. Yen and F.T. Huang. The use of PET imaging for prognostic integrin alpha2beta1 phenotyping to detect non-small cell lung cancer and monitor drug resistance responses. *Theranostics* 7: 4013–4028, 2017.

Huang, J.S., C.J. Yao, S.E. Chuang, C.T. Yeh, L.M. Lee, R.M. Chen, W.J. Chao, J. Whang-Peng and G.M. Lai. Honokiol inhibits sphere formation and xenograft growth of oral cancer side population cells accompanied with JAK/STAT signaling pathway suppression and apoptosis induction. *BMC Cancer* 16: 245, 2016.

Huang, W.C., K.T. Kuo, O.A. Bamodu, Y.K. Lin, C.H. Wang, K.Y. Lee, L.S. Wang, C.T. Yeh and J. T. Tsai. Astragalus polysaccharide (PG2) ameliorates cancer symptom clusters, as well as improves quality of life in patients with metastatic disease, through modulation of the inflammatory cascade. *Cancers (Basel)* 11: 2019.

Hurst, D.R. and D.R. Welch. Metastasis suppressor genes at the interface between the environment and tumor cell growth. *Int. Rev. Cell Mol. Biol.* 286: 107–180, 2011.

Jiang, Y.N., H.Q. Yan, X.B. Huang, Y.N. Wang, Q. Li and F.G. Gao. Interleukin 6 trigged ataxia-telangiectasia mutated activation facilitates lung cancer metastasis via MMP-3/MMP-13 up-regulation. *Oncotarget* 6: 40719–40733, 2015.

Jin, M., K. Zhao, Q. Huang and P. Shang. Structural features and biological activities of the polysaccharides from Astragalus membranaceus. *Int. J. Biol. Macromol.* 64: 257–266, 2014.

Keibel, A., V. Singh and M.C. Sharma. Inflammation, microenvironment, and the immune system in cancer progression. *Curr. Pharm. Des.* 15: 1949–1955, 2009.

Keshamouni, V.G., P. Jagtap, G. Michailidis, J.R. Strahler, R. Kuick, A.K. Reka, P. Papoulias, R. Krishnapuram, A. Srirangam, T.J. Standiford, P.C. Andrews and G.S. Omenn. Temporal quantitative proteomics by iTRAQ 2D-LC-MS/MS and corresponding mRNA expression analysis identify post-transcriptional modulation of actin-cytoskeleton regulators during TGF-beta-Induced epithelial-mesenchymal transition. *J. Proteome Res.* 8: 35–47, 2009.

Kolak, A., M. Kaminska, E. Wysokinska, D. Surdyka, D. Kieszko, M. Pakiela and F. Burdan. The problem of fatigue in patients suffering from neoplastic disease. *Contemp. Oncol. (Pozn)* 21: 131–135, 2017.

Koorstra, J.B., C.A. Karikari, G. Feldmann, S. Bisht, P.L. Rojas, G.J. Offerhaus, H. Alvarez and A. Maitra. The Axl receptor tyrosine kinase confers an adverse prognostic influence in pancreatic cancer and represents a new therapeutic target. *Cancer Biol. Ther.* 8: 618–626, 2009.

Kuo, Y.L., C.H. Chen, T.H. Chuang, W.K. Hua, W.J. Lin, W.H. Hsu, P.M. Chang, S.L. Hsu, T.H. Huang, C.Y. Kao and C.Y. Huang. Gene expression profiling and pathway network analysis predicts a novel antitumor function for a botanical-derived drug, PG2. *Evid. Based Complement. Alternat. Med.* 2015: 917345, 2015.

Lamouille, S., J. Xu and R. Derynck. Molecular mechanisms of epithelial-mesenchymal transition. *Nat. Rev. Mol. Cell Biol.* 15: 178–196, 2014.

Lay, J.D., C.C. Hong, J.S. Huang, Y.Y. Yang, C.Y. Pao, C.H. Liu, Y.P. Lai, G.M. Lai, A.L. Cheng, I. J. Su and S.E. Chuang. Sulfasalazine suppresses drug resistance and invasiveness of lung adenocarcinoma cells expressing AXL. *Cancer Res.* 67: 3878–3887, 2007.

Lopez-Novoa, J.M. and M.A. Nieto. Inflammation and EMT: An alliance towards organ fibrosis and cancer progression. *EMBO Mol. Med.* 1: 303–314, 2009.

McKenna, D., K. Hughes and K. Jones. Astragalus. *Altern. Ther. Health Med.* 8: 34–40; quiz 41–32, 124, 2002.

Mishra, A., J. Wang, Y. Shiozawa, S. McGee, J. Kim, Y. Jung, J. Joseph, J.E. Berry, A. Havens, K.J. Pienta and R.S. Taichman. Hypoxia stabilizes GAS6/Axl signaling in metastatic prostate cancer. *Mol. Cancer Res.* 10: 703–712, 2012.

Mittal, V. Epithelial mesenchymal transition in tumor metastasis. *Annu. Rev. Pathol.* 13: 395–412, 2018.

Myers, J.S. Proinflammatory cytokines and sickness behavior: Implications for depression and cancer-related symptoms. *Oncol. Nurs. Forum* 35: 802–807, 2008.

Nishihira, J., T. Ishibashi, T. Fukushima, B. Sun, Y. Sato and S. Todo. Macrophage migration inhibitory factor (MIF): Its potential role in tumor growth and tumor-associated angiogenesis. *Ann. N. Y. Acad. Sci.* 995: 171–182, 2003.

Ohkawara, T., J. Nishihira, H. Takeda, S. Hige, M. Kato, T. Sugiyama, T. Iwanaga, H. Nakamura, Y. Mizue and M. Asaka. Amelioration of dextran sulfate sodium-induced colitis by anti-macrophage migration inhibitory factor antibody in mice. *Gastroenterology* 123: 256–270, 2002.

Onodera, S., J. Nishihira, K. Iwabuchi, Y. Koyama, K. Yoshida, S. Tanaka and A. Minami. Macrophage migration inhibitory factor up-regulates matrix metalloproteinase-9 and -13 in rat osteoblasts. Relevance to intracellular signaling pathways. *J. Biol. Chem.* 277: 7865–7874, 2002.

Otvos, B., D.J. Silver, E.E. Mulkearns-Hubert, A.G. Alvarado, S.M. Turaga, M.D. Sorensen, P. Rayman, W.A. Flavahan, J.S. Hale, K. Stoltz, M. Sinyuk, Q. Wu, A. Jarrar, S.H. Kim, P.L. Fox, I. Nakano, J.N. Rich, R.M. Ransohoff, J. Finke, B.W. Kristensen, M.A. Vogelbaum and J.D. Lathia. Cancer stem cell-secreted macrophage migration inhibitory factor stimulates myeloid derived suppressor cell function and facilitates glioblastoma immune evasion. *Stem Cells* 34: 2026–2039, 2016.

Pan, X., X. Mao, T. Cheng and X. Zhang. Macrophage migration inhibitory factor: A regulator of MMP13 and inflammation in titanium particles-stimulated air pouch in vivo. *Mol. Cell Biochem.* 357: 313–321, 2011.

Phacharapiyangkul, N., L.H. Wu, W.Y. Lee, Y.H. Kuo, Y.J. Wu, H.P. Liou, Y.E. Tsai and C.H. Lee. The extracts of Astragalus membranaceus enhance chemosensitivity and reduce tumor indoleamine 2, 3-dioxygenase expression. *Int. J. Med. Sci.* 16: 1107–1115, 2019.

Rendon, B.E., T. Roger, I. Teneng, M. Zhao, Y. Al-Abed, T. Calandra and R.A. Mitchell. Regulation of human lung adenocarcinoma cell migration and invasion by macrophage migration inhibitory factor. *J. Biol. Chem.* 282: 29910–29918, 2007.

Salaun, M., J. Peng, H.H. Hensley, N. Roder, D.B. Flieder, S. Houlle-Crepin, O. Abramovici-Roels, J.C. Sabourin, L. Thiberville and M.L. Clapper. MMP-13 in-vivo molecular imaging reveals early expression in lung adenocarcinoma. *PLoS One* 10: e0132960, 2015.

Torre, L.A., R.L. Siegel and A. Jemal. Lung cancer statistics. *Adv. Exp. Med. Biol.* 893: 1–19, 2016.

Tsai, J.H. and J. Yang. Epithelial-mesenchymal plasticity in carcinoma metastasis. *Genes Dev.* 27: 2192–2206, 2013.

White, E.S., K.R. Flaherty, S. Carskadon, A. Brant, M.D. Iannettoni, J. Yee, M.B. Orringer and D.A. Arenberg. Macrophage migration inhibitory factor and CXC chemokine expression in non-small cell lung cancer: Role in angiogenesis and prognosis. *Clin. Cancer Res.* 9: 853–860, 2003.

Winner, M., J. Meier, S. Zierow, B.E. Rendon, G.V. Crichlow, R. Riggs, R. Bucala, L. Leng, N. Smith, E. Lolis, J.O. Trent and R.A. Mitchell. A novel, macrophage migration inhibitory factor suicide substrate inhibits motility and growth of lung cancer cells. *Cancer Res.* 68: 7253–7257, 2008.

Wu, F., J. Li, C. Jang, J. Wang and J. Xiong. The role of Axl in drug resistance and epithelial-to-mesenchymal transition of non-small cell lung carcinoma. *Int. J. Clin. Exp. Pathol.* 7: 6653–6661, 2014.

Xu, X., B. Wang, C. Ye, C. Yao, Y. Lin, X. Huang, Y. Zhang and S. Wang. Overexpression of macrophage migration inhibitory factor induces angiogenesis in human breast cancer. *Cancer Lett.* 261: 147–157, 2008.

Youn, H., B. Son, W. Kim, S.Y. Jun, J.S. Lee, J.M. Lee, C. Kang, J. Kim and B. Youn. Dissociation of MIF-rpS3 complex and sequential NF-kappaB activation is involved in IR-induced metastatic conversion of NSCLC. *J. Cell Biochem.* 116: 2504–2516, 2015.

Zhang, G., X. Kong, M. Wang, H. Zhao, S. Han, R. Hu, J. Huang and W. Cui. AXL is a marker for epithelial-mesenchymal transition in esophageal squamous cell carcinoma. *Oncol. Lett.* 15: 1900–1906, 2018.

Zhang, G., M. Wang, H. Zhao and W. Cui. Function of Axl receptor tyrosine kinase in non-small cell lung cancer. *Oncol. Lett.* 15: 2726–2734, 2018.